nature physics

ARTICLES

PUBLISHED ONLINE: 28 AUGUST 2017 | DOI: 10.1038/NPHYS4243

Four-body ring-exchange interactions and anyonic statistics within a minimal toric-code Hamiltonian

Han-Ning Dai[1,2,3†], Bing Yang[1,2,3†], Andreas Reingruber[2,4], Hui Sun[1,3], Xiao-Fan Xu[2], Yu-Ao Chen[1,3,5], Zhen-Sheng Yuan[1,2,3,5*] and Jian-Wei Pan[1,2,3,5*]

Ring exchange is an elementary interaction for modelling unconventional topological matter. Here, we report the observation of four-body ring-exchange interactions and the topological properties of anyonic excitations within an ultracold atom system. A minimum toric-code Hamiltonian, in which the ring exchange is the dominant term, was implemented in disconnected four-spin plaquette arrays formed by two orthogonal superlattices. The ring-exchange interactions were resolved from the dynamical evolutions of the spin orders in each plaquette, matching well with the predicted energy gaps between two anyonic excitations of the spin system. A braiding operation was applied to the spins in the plaquettes and an induced phase 1.00(3)π in the four-spin state was observed, confirming 1/2 mutual statistics. This work offers new prospects for the quantum simulation of topological phases by engineering many-body interactions.

Exploiting the laws of quantum mechanics, quantum information processing can be exponentially faster than its classical counterpart[1]. To make this technology a reality, scientists have to solve the crucial problem of decoherence and systematic errors in real quantum systems, which is very difficult due to the requirement for an extremely small error threshold to enable error corrections[2,3]. An encouraging solution to this problem is the Kitaev toric model[4] by taking advantage of anyons, a sort of topological quasiparticles being neither bosons nor fermions[5]. In this model, anyons are exploited to encode and manipulate information in a manner which is resistant to errors, the so-called topological protection. Schemes for simulating the Kitaev model with different systems such as photons[6], ions[7], superconducting circuits[8], and ultracold atoms[9–16] have been proposed. In experiments, non-interacting systems were used to solely mimic the anyonic statistics through braiding operations[17–20]. Furthermore, the toric-code interaction has been simulated by a digital quantum simulator composed of ions through dissipative pumping processes[21]. However, because the background four-body ring-exchange interacting Hamiltonian[9,10] does not exist in these systems, they cannot protect from noises due to lack of an energy gap and it is not possible to unambiguously define the anyonic excitations[22].

Interacting ultracold atoms in optical lattices, which can be well described by the Hubbard models[23], are regarded as a promising system for simulating many-body physics[24]. By engineering the Hubbard parameters, one can gain valuable insights from experimental studies of the one-dimensional Ising and Heisenberg chains[25,26], the resonating valence-bond (RVB) states in local plaquettes[27], the Harper–Hofstadter and Haldane models[28–30], as well as the quantum entanglement properties between atoms[31–33], and so on. However, the ring-exchange interaction, which is relevant to the toric-code model[9] and the quantum link models of $U(1)$ lattice gauge theory[10], remains notoriously difficult to implement in experiment due to the nature of its fourth-order spin interaction. It is usually greatly suppressed compared to the lower-order processes, such as superexchange interactions[34,35].

To experimentally investigate the ring-exchange interactions, a practical scheme[9] was proposed with ultracold atoms in optical lattices by suppressing the second-order interactions. Following this proposal[9], we first built disconnected four-site plaquettes, whose sites are singly occupied by atomic spins, through constructing a two-dimensional (2D) squared optical superlattice. By carefully suppressing the superexchange interactions between atomic spins in neighbouring sites with an effective gradient field, the interaction among the four spins is then dominated by the ring-exchange interaction. This high-order interaction was observed by measuring the dynamical evolution of atomic spin configurations in the plaquettes. Furthermore, making use of the ring-exchange Hamiltonian, we experimentally demonstrate the fractional statistics of Abelian anyons[4] by a braiding operation and an interference process.

The system under consideration is a four-site plaquette singly occupied with four bosonic atoms in two internal states $|\downarrow\rangle$ and $|\uparrow\rangle$ (Fig. 1a). It can be well described by a two-species single-band Bose–Hubbard model (BHM), characterized by the tunnelling matrix element $J_{x(y)}$ along the $x(y)$ direction, an on-site interaction U and the spin-dependent intra-plaquette gradient $\Delta_{x(y)}$. In the regime of strong interactions $J_{x(y)} \ll U$ and $4J_{x(y)}^2/U \ll \Delta_{x(y)}$, both the bare tunnelling and the superexchange interactions are suppressed, while the fourth-order ring-exchange interactions become dominant. Hence the four-site Hubbard Hamiltonian is reduced to (see Supplementary Methods and ref. 9)

$$\hat{H}_{\mathrm{R}} = -J_{\square}(\hat{S}_1^+\hat{S}_2^-\hat{S}_3^+\hat{S}_4^- + \mathrm{H.c.}) - J_+\sum_{\langle j,k\rangle}\hat{S}_j^z\hat{S}_k^z + \sum_j \Delta_j\hat{S}_j^z \qquad (1)$$

[1]Hefei National Laboratory for Physical Sciences at Microscale and Department of Modern Physics, University of Science and Technology of China, Hefei, Anhui 230026, China. [2]Physikalisches Institut, Ruprecht-Karls-Universität Heidelberg, Im Neuenheimer Feld 226, 69120 Heidelberg, Germany. [3]CAS Centre for Excellence and Synergetic Innovation Centre in Quantum Information and Quantum Physics, University of Science and Technology of China, Hefei, Anhui 230026, China. [4]Department of Physics and Research Center OPTIMAS, University of Kaiserslautern, Erwin-Schroedinger-Strasse, Building 46, 67663 Kaiserslautern, Germany. [5]CAS-Alibaba Quantum Computing Laboratory, Shanghai 201315, China. †These authors contributed equally to this work. *e-mail: yuanzs@ustc.edu.cn; pan@ustc.edu.cn

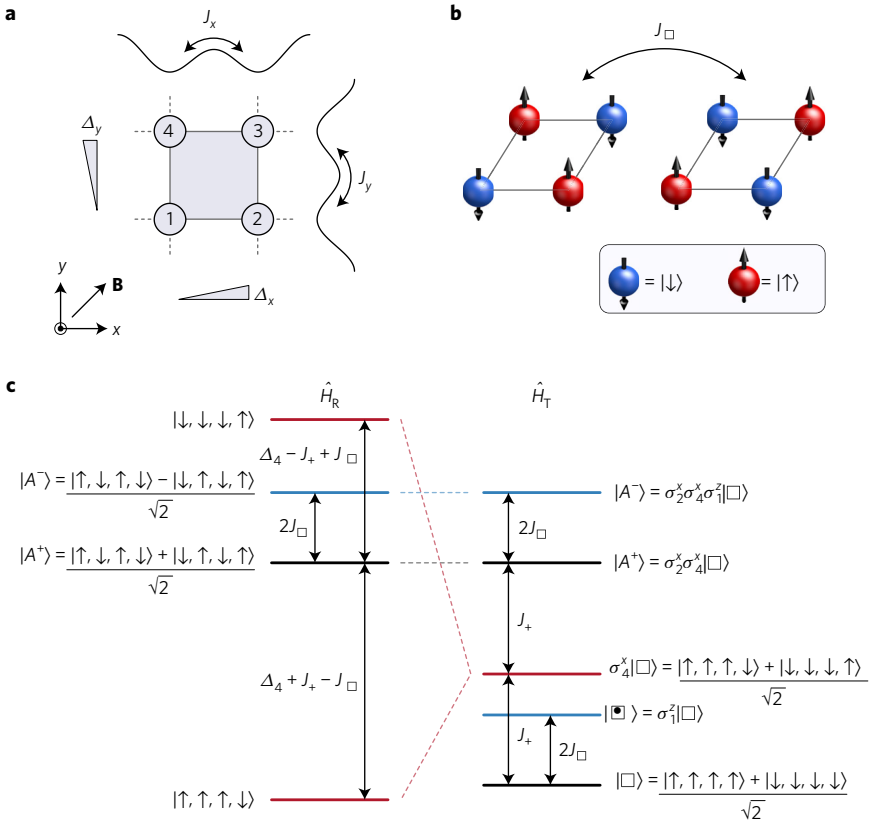

Figure 1 | Experimental scheme and the ring-exchange process in disconnected four-site plaquettes. a, Isolated optical plaquettes with effective magnetic gradients are created by two orthogonal spin-dependent superlattices, and the sites of each plaquette are enumerated in a counter-clockwise fashion. **b**, The ring-exchange-driven oscillations take place between the two antiferromagnetically ordered states $|\uparrow,\downarrow,\uparrow,\downarrow\rangle$ and $|\downarrow,\uparrow,\downarrow,\uparrow\rangle$. **c**, The eigenstates and related energies for modelling a minimal instance of the toric-code model $\hat{H}_T$ with the ring-exchange dominating Hamiltonian $\hat{H}_R$ in an optical plaquette.

in which $J_\square \approx 40J_x^2J_y^2/U^3$ describes the effective ring-exchange interaction arising from a fourth-order tunnelling process, $J_+ \approx 4J_{x(y)}^2/U$ denotes a nearest-neighbour Ising-type interaction along the $x(y)$ direction, and Δ_j are the spin-dependent potential biases on site j. Therefore, the intra-plaquette gradients along the two directions are defined as $\Delta_x = \Delta_2 - \Delta_1$ and $\Delta_y = \Delta_4 - \Delta_1$. The corresponding spin operators are defined through the bosonic creation and annihilation operators $\hat{a}_{\sigma,j}^\dagger$ and $\hat{a}_{\sigma,j}$ as $\hat{S}_j^+ = \hat{a}_{\uparrow,j}^\dagger\hat{a}_{\downarrow,j}$, $\hat{S}_j^- = \hat{a}_{\downarrow,j}^\dagger\hat{a}_{\uparrow,j}$ and $\hat{S}_j^z = (\hat{a}_{\uparrow,j}^\dagger\hat{a}_{\uparrow,j} - \hat{a}_{\downarrow,j}^\dagger\hat{a}_{\downarrow,j})/2$, with the two spin states $\sigma = \uparrow, \downarrow$. Due to the spatial symmetry of the Hamiltonian, the ring-exchange process can take place only between the two antiferromagnetically ordered states: $|\downarrow,\uparrow,\downarrow,\uparrow\rangle$ and $|\uparrow,\downarrow,\uparrow,\downarrow\rangle$, where the commas separate the occupations of the four sites. Therefore, a system initialized to $|\downarrow,\uparrow,\downarrow,\uparrow\rangle$ will evolve to $|\uparrow,\downarrow,\uparrow,\downarrow\rangle$ under the ring-exchange dominating Hamiltonian, and vice versa (Fig. 1b). This process can be effectively described with the representation of Bloch sphere in a two-level system of $\mathbb{H}: \{|\uparrow,\downarrow,\uparrow,\downarrow\rangle, |\downarrow,\uparrow,\downarrow,\uparrow\rangle\}$, with $|A^\pm\rangle = (|\uparrow,\downarrow,\uparrow,\downarrow\rangle \pm |\downarrow,\uparrow,\downarrow,\uparrow\rangle)/\sqrt{2}$ set as $\pm\hat{e}_x$, $(|\uparrow,\downarrow,\uparrow,\downarrow\rangle \pm i|\downarrow,\uparrow,\downarrow,\uparrow\rangle)/\sqrt{2}$ as $\pm\hat{e}_y$, and $|\uparrow,\downarrow,\uparrow,\downarrow\rangle/|\downarrow,\uparrow,\downarrow,\uparrow\rangle$ set as $\pm\hat{e}_z$, respectively. Therefore, the energy separation of $2J_\square$ between the two eigenstates of H_R (Fig. 1c), that is, $|A^+\rangle$ and $|A^-\rangle$, sets the evolution frequency of the coherent ring-exchange dynamics in the yz-plane of the Bloch sphere. We use the projection along the z-axis of the Bloch sphere (the spin imbalance), $N_z = \langle\hat{S}_1^z - \hat{S}_2^z + \hat{S}_3^z - \hat{S}_4^z\rangle/2$, to characterize the ring-exchange dynamics. Here, $\langle\hat{S}_j^z\rangle$ denote the corresponding quantum mechanical expectation values of $\hat{S}^z$ on site j.

To study the four-body ring-exchange interactions, we initially prepare an ultracold ensemble of ^{87}Rb atoms with two relevant internal states $|\downarrow\rangle = |F=1, m_F=-1\rangle$ and $|\uparrow\rangle = |F=2, m_F=-2\rangle$ in a 2D array of disconnected plaquettes into an antiferromagnetically ordered configuration $|\downarrow,\uparrow,\downarrow,\uparrow\rangle$ (Fig. 2a). The state initialization is started by preparing a 2D Mott insulator in a square lattice[33]. Thereafter, the plaquette potentials are generated by two orthogonal spin-dependent superlattices in the xy plane. Each of them is created by overlapping two standing waves with periods of 383.5 nm (short lattice) and 767 nm (long lattice) with a balanced structure. The depths of the short lattices (V_{xs} and V_{ys}) and long lattices (V_{xl} and V_{yl}) are given in units of the recoil energy $E_r = h^2/(2m\lambda^2)$, where $\lambda = 767$ nm, m is the mass of the atom and h is the Planck constant. With a bias magnetic field of 1.39 G along the $\hat{x}+\hat{y}$ direction, we use a resonant microwave (MW) field ~6.8 GHz to couple the spin states $|\downarrow\rangle$ and $|\uparrow\rangle$. The degeneracy of the transitions $|\downarrow\rangle \rightarrow |\uparrow\rangle$ on each plaquette site is removed by setting the lattice depths $V_{xs} = V_{ys} = 150(1)\ E_r$, $V_{xl} = V_{yl} = 56.3(4)\ E_r$ and tuning the short-lattice polarization (with an intersecting angle of $\pi/3$ between the polarizations of the incident and retro-reflected beams, see Supplementary Methods). Thereby a spin-dependent potential is created, as $\Delta_1 = -32.6(1)$ kHz, $\Delta_3 = 32.6(1)$ kHz, and $\Delta_2 = \Delta_4 = 0$. Hence, we selectively transfer the atoms on sites 2 and 4 into $|\uparrow\rangle$ via a resonant MW π-pulse of 60.5 μs (Fig. 2a). As a result, the spin configuration in every plaquette is initialized to the antiferromagnetically ordered state $|\downarrow,\uparrow,\downarrow,\uparrow\rangle$ in parallel. An overall state initialization efficiency of 92(2)% is derived by applying another addressing π-pulse after 200 ms holding in the lattice, and measuring the residual atoms on $|\uparrow\rangle$. The same selective addressing procedure is used in the spin-imbalance measurement in the later experiment.

The four-spin dynamics can be controlled by the tunnelling parameters $J_{x(y)}$, the on-site interactions U and the intra-plaquette

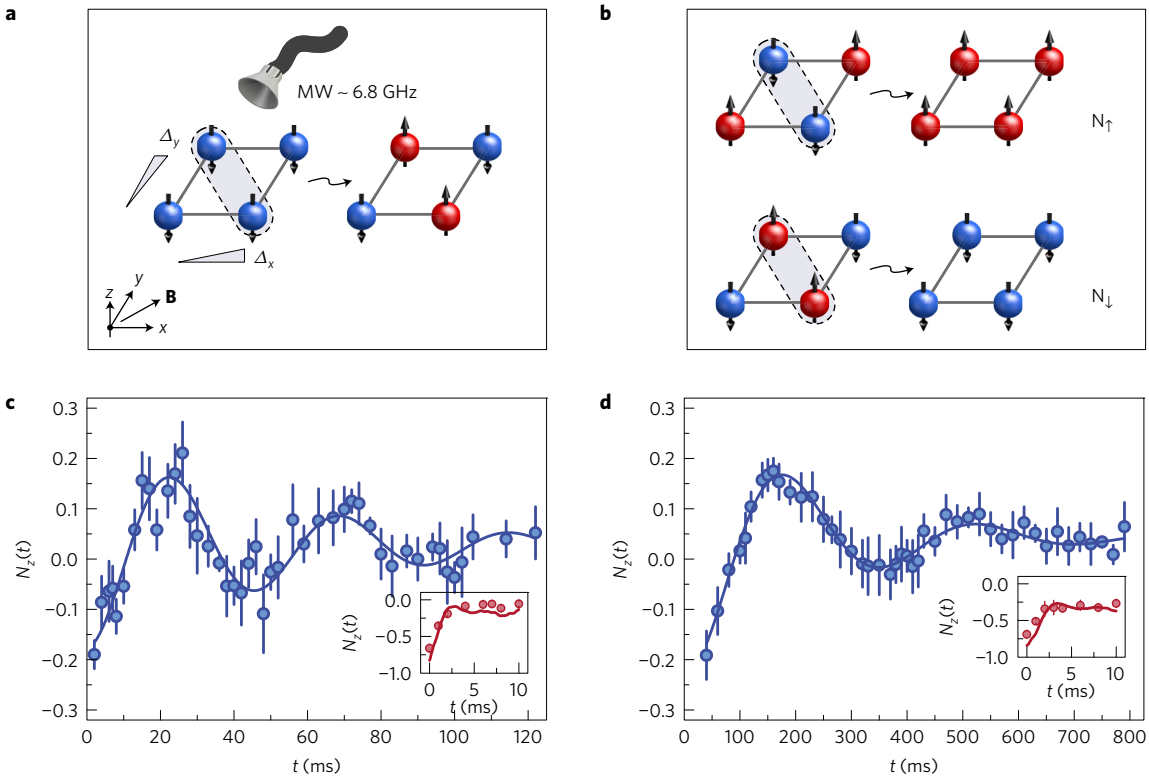

Figure 2 | Observation of four-body ring-exchange interactions. a, A spin-dependent potential lifts the degeneracy of spins on the four sites. The system is initialized from $|\downarrow,\downarrow,\downarrow,\downarrow\rangle$ to $|\downarrow,\uparrow,\downarrow,\uparrow\rangle$ by selectively addressing site 2 and 4 with a MW field. **b**, Spin configurations are read out by first addressing and flipping the sites 2 and 4, and then imaging the two spin components by taking two *in situ* absorption images $N_\uparrow(x,y)$ and $N_\downarrow(x,y)$ in sequence. **c**,**d**, Measured spin dynamics of $N_z(t)$ (blue circles) in isolated plaquettes in the presence of an effective magnetic gradient are shown for two different settings: $V_{xs}=16.7(1)\,E_r$, $V_{ys}=17.2(1)\,E_r$, $U=894$ Hz, $J_x/U=0.12$, $J_y/U=0.11$ (**c**); and $V_{xs}=19.2(1)\,E_r$, $V_{ys}=18.2(1)\,E_r$, $U=953$ Hz, $J_x/U=0.064$, $J_y/U=0.075$ (**d**). The measured data for spin imbalance are fitted with a damped sine wave (blue lines). Shown in the insets are the fast decay processes in the beginning of the dynamics (red circles), matching well the theoretical predictions by including the number of vacancies in the lattice (red lines). The error bars denote statistical errors, which are 1 s.d.

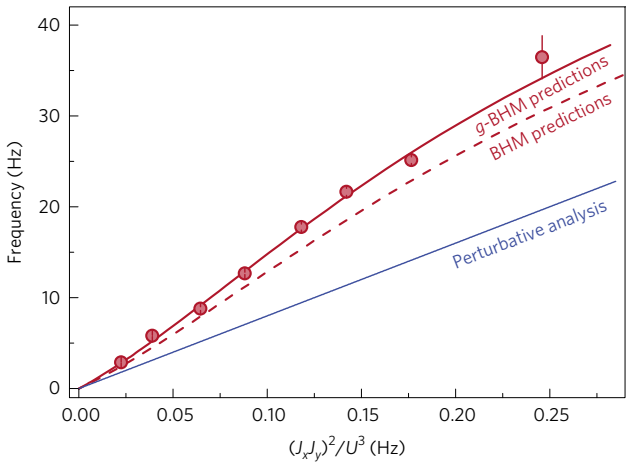

Figure 3 | Frequencies of the spin oscillations. The major frequencies obtained by fitting the spin imbalanced data for various values of V_{xs} and V_{ys} (red circles) are compared to the theoretical predictions of the perturbative analysis (blue solid line), the standard BHM (red dashed line) and the generalized BHM (red solid line). Error bars denote the uncertainties obtained from the fitting results.

gradients $\Delta_{x(y)}$. We first ramp down the long lattices to 10 E_r, and set $\Delta_x=115(1)$ Hz, $\Delta_y=145(1)$ Hz. Then the four-spin dynamics in the plaquette is initiated by rapidly ramping down the short lattices from 60 E_r to lower depths within 500 μs. After letting the system evolve for a time t, we halt the ring-exchange-driven dynamics and freeze the spin configurations by simultaneously ramping up the short lattices to 150 E_r in 1.5 ms. We detect the four-spin configurations by applying a site-resolved spin flipping operation, and taking two absorption images $N_\uparrow(x,y)$ and $N_\downarrow(x,y)$ in sequence (Fig. 2b). The two plaquette configurations $|\uparrow,\downarrow,\uparrow,\downarrow\rangle$ and $|\downarrow,\uparrow,\downarrow,\uparrow\rangle$ are respectively recorded. Therefore, the spin imbalance can be derived by

$$N_z=\frac{\sum_{\mathrm{ROI}}(N_\uparrow(x,y)-N_\downarrow(x,y))}{\sum_{\mathrm{ROI}}(N_\uparrow(x,y)+N_\downarrow(x,y))} \quad (2)$$

where a region of interest (ROI) in the centre of the atom cloud containing about 272 plaquettes is selected for data analysis.

Two typical evolution curves are shown in Fig. 2c,d, where the slow oscillations of $N_z(t)$ reveal the corresponding four-body ring-exchange interactions. A ring-exchange oscillation frequency of 21.6(4) Hz is obtained under the Hubbard parameters $J_x/U=0.12$, $J_y/U=0.11$. The emergence of some higher-frequency components indicates that the lower-order processes have not been fully suppressed. Increasing the barriers of the plaquette, a lower ring-exchange frequency of 2.9(1) Hz is derived under the condition of $J_x/U=0.064$, $J_y/U=0.075$, where the oscillation becomes smoother and the higher-frequency components become invisible. The finite amplitudes 0.26(3) of the oscillations are mainly limited by the Mott filling properties, which give rise to ~0.37 of the full amplitude. Further reductions can be explained by imperfections in the efficiencies of the microwave addressing operations and the

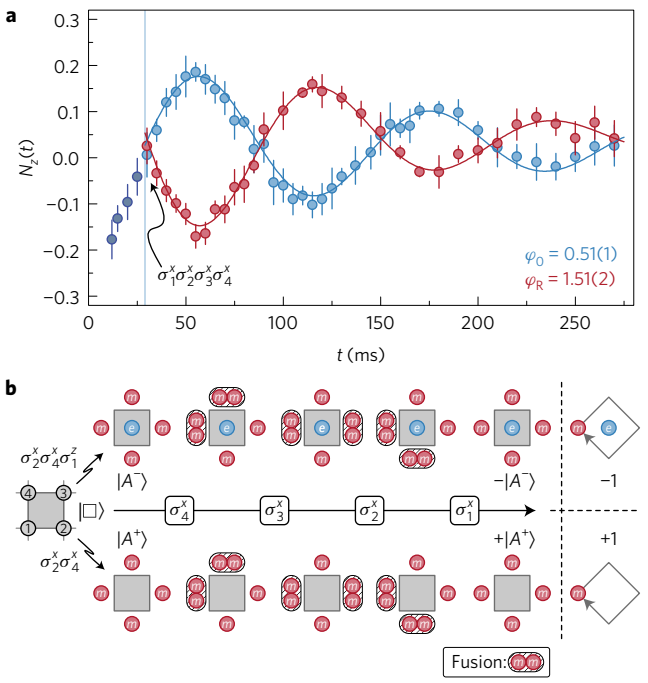

Figure 4 | Coherent control of ring-exchange dynamics and braiding anyons in a minimal toric-code model. a, Two distinct ring-exchange-driven evolutions of the spin imbalance with (red circles) and without (blue circles) implementing the global state operation $\sigma_1^x\sigma_2^x\sigma_3^x\sigma_4^x$ at $T/4$ are measured, under the setting of $V_{xs} = 18.2(1)\ E_r$, $V_{ys} = 17.2(1)\ E_r$, $U = 919$ Hz, $J_x/U = 0.082$, $J_y/U = 0.10$, $T = 117(1)$ ms. Fitting the results with damped sine waves (red and blue lines) and comparing the phase parameters, a relative phase shift of $\Delta\varphi = 1.00(3)\pi$ is derived after the $\sigma_1^x\sigma_2^x\sigma_3^x\sigma_4^x$ operation. The error bars denote statistical errors, which are 1 s.d. **b**, The braiding operation on quasiparticles: first two *m*-particles (red circles) are created by σ_4^x; then a single *m*-particle is moved around the plaquette by subsequent application of σ_3^x, σ_2^x and σ_1^x; in the end, the two *m*-particles are annihilated. For the case with the presence of an *e*-particle in the plaquette, $|A^-\rangle$, the system picks up a nontrivial phase factor of −1. While for the case without *e*-particles, $|A^+\rangle$, no additional phase is acquired.

suppression of the lower-order processes. The background noises caused by the plaquettes with defects decay to a steady value of N_z at the beginning of evolution through the bare tunnelling processes (see insets in Fig. 2c,d and Supplementary Methods). The damping of the ring-exchange oscillations is induced by coupling with other states which are not in the subspace of $\mathbb{H}$, as well as dephasing caused by spatial inhomogeneities of the coupling parameters within the ensemble.

The four-body ring-exchange evolutions are measured at varying parameters as shown in Fig. 3, with the oscillation frequencies ranging from 2.9(1) Hz to 36(2) Hz. The deviation of the experimental data from the perturbation analysis can be mainly attributed to the imperfect suppression of the lower-order processes in the standard BHM. However, additional modifications of the density-induced tunnelling, nearest-neighbour interactions and pair tunnelling terms will further enhance the effective ring-exchange term by 12–15% (see Supplementary Methods). These effects form the generalized Bose–Hubbard model (g-BHM)[36]. A comparison between the experiment and the theoretical predictions of the g-BHM results in excellent agreement, which confirms that the dominant dynamics observed here is the four-body ring-exchange process.

Furthermore, we demonstrate coherent control of the ring-exchange-driven dynamics by applying a global state operation $\sigma_1^x\sigma_2^x\sigma_3^x\sigma_4^x$ during the evolution. This operation creates a phase on the two ring-exchange-related eigenstates as $\sigma_1^x\sigma_2^x\sigma_3^x\sigma_4^x|A^\pm\rangle = \pm|A^\pm\rangle$, which can be derived from a phase shift in the dynamical evolution of the spin orders[9,11]. Concretely, after initializing the system to $|\downarrow,\uparrow,\downarrow,\uparrow\rangle$ in the experiment, we let the system evolve to a superposition state $(|A^+\rangle + i|A^-\rangle)/\sqrt{2}$ through a quarter-period of ring-exchange oscillation (Fig. 4a), where the phase i is a relative phase. Then a single-frequency MW π-pulse of 19 μs with a Rabi frequency of $\Omega = 26.3$ kHz is applied to flip every site on the plaquette, which is equivalent to performing the global operation $\sigma_1^x\sigma_2^x\sigma_3^x\sigma_4^x$ on the four-spin states. The efficiency of the π-pulse for each site is close to unity, as $\Delta_{x(y)} \ll \Omega$. The state $|A^-\rangle$ picks up an additional phase factor −1, and the system ends up in $(|A^+\rangle - i|A^-\rangle)/\sqrt{2}$. Afterwards, the state evolves under the same ring-exchange setting and the dynamical evolution is recorded (Fig. 4a). A relative phase shift $\Delta\varphi = \varphi_R - \varphi_0 = 1.00(3)\pi$ can be obtained by comparing the two oscillations with and without implementing the global spin flipping. Thus one gets a resulting phase factor $e^{i\Delta\varphi} = -1.00(3)$ acquired on $|A^-\rangle$ after applying $\sigma_1^x\sigma_2^x\sigma_3^x\sigma_4^x$. This clearly reveals again that the ring-exchange dynamics are well described by the two eigenstates $|A^\pm\rangle$.

By utilizing the well-controlled ring-exchange dominating Hamiltonian in our experiment, we can implement a minimal instance of Kitaev's toric-code model[9]. Within the subspace of $\mathbb{H}$, the Hamiltonian $\hat{H}_R$ (equation (1)) is equivalent to

$$\hat{H}_T = -J_\square\sigma_1^x\sigma_2^x\sigma_3^x\sigma_4^x - \frac{J_+}{4}\sum_{\langle j,k\rangle}\sigma_j^z\sigma_k^z \qquad (3)$$

where $\sigma_j^{x(z)}$ are the Pauli operators on site j. It can be regarded as a quantum link model of $U(1)$ lattice gauge theory[10,13] as well. The first term of this Hamiltonian corresponds to the ring-exchange interactions, while the second term of four two-body Ising terms is reduced from the four-body Ising vertex terms of the toric-code model due to the geometry of an isolated four-site plaquette. The ground state of this model takes the form $|\square\rangle = (|\uparrow,\uparrow,\uparrow,\uparrow\rangle + |\downarrow,\downarrow,\downarrow,\downarrow\rangle)/\sqrt{2}$, while the first excited state with an energy of $2J_\square$ is $|\boxdot\rangle = (|\uparrow,\uparrow,\uparrow,\uparrow\rangle - |\downarrow,\downarrow,\downarrow,\downarrow\rangle)/\sqrt{2}$ (see Fig. 1c). It can be generated in principle by applying, for example, the σ_1^z operation to the ground state, and is known as a quasiparticle of 'electric charge' (*e*-particle). Another type of excitation with an energy of J_+ can be generated by applying a single-qubit rotation on the ground state, for example, $\sigma_4^x|\square\rangle = (|\uparrow,\uparrow,\uparrow,\downarrow\rangle + |\downarrow,\downarrow,\downarrow,\uparrow\rangle)/\sqrt{2}$, which actually excites a pair of so-called 'magnetic vortices' (*m*-particles). In this minimal toric-code model, the two antiferromagnetically ordered states $|A^\pm\rangle$ are energetically high-lying eigenstates (see Fig. 1c and Supplementary Methods), that is, $|A^+\rangle = \sigma_2^x\sigma_4^x|\square\rangle$ and $|A^-\rangle = \sigma_2^x\sigma_4^x\sigma_1^z|\square\rangle$. Hence, there are four *m*-particles existing on the four edges of the plaquette in $|A^+\rangle$, while an additional *e*-particle lives at the centre of the plaquette in $|A^-\rangle$ (ref. 9). On the basis of the fusion rules[4], when two anyons of the same type are created at the same position, they annihilate[18]. For example, $\sigma_1^x\sigma_1^x|\square\rangle = |\square\rangle$.

We then analyse anyonic fractional statistics of quasiparticles in this minimal toric code. Specifically, the global state operation $\sigma_1^x\sigma_2^x\sigma_3^x\sigma_4^x$ in the above experiment is equivalent to a braiding operation $\sigma_1^x\sigma_2^x\sigma_3^x\sigma_4^x$, which can be described as: first creating a pair of *m*-particles on the two edges of the plaquette, then cyclically moving one *m*-particle around the plaquette, and annihilating the two *m*-particles in the end (see Fig. 4b). For the case with the presence of an *e*-particle in the plaquette, $|A^-\rangle$, the system picks up a nontrivial phase factor of −1. While for the case without *e*-particles, $|A^+\rangle$, no additional phase is acquired. The nontrivial phase factor of −1 acquired after the braiding operations denotes the presence of relative 1/2-anyons in $|A^-\rangle$. It can be clearly seen from the braiding process that additional energy levels out of the subspace $\mathbb{H}$ are

involved, for example, $\sigma_4^x|A^-\rangle = (|\uparrow,\downarrow,\uparrow,\uparrow\rangle - |\downarrow,\uparrow,\downarrow,\downarrow\rangle)/\sqrt{2}$ with an energy difference of J_+ comparing to $|A^-\rangle$ and resulting in annihilation of a pair of m-particles. Obviously, the Bloch sphere representation is no longer sufficient to describe the physics of the braiding process. The observed dynamical phase difference is an unambiguous signature of fractional statistics.

In summary, we have engineered the Hubbard parameters of a plaquette system and isolated a minimum instance of the toric-code Hamiltonian from a lattice system. The ring-exchange interaction has been observed by controlling and measuring dynamical oscillations between the spin configurations $|\downarrow,\uparrow,\downarrow,\uparrow\rangle$ and $|\uparrow,\downarrow,\uparrow,\downarrow\rangle$. Applying a braiding operation to the plaquette state, we found a statistical phase of π, demonstrating the exotic fractional statistics of Abelian anyons. Optimizing the filling parameters in the Mott insulator state by novel cooling and loading techniques[37,38] will give rise to plaquette arrays with fewer defects and ring-exchange dynamics with higher contrasts. To achieve stronger ring-exchange strengths, one may use lighter atoms (say, lithium) to enhance the tunnelling while using tighter traps and exploiting Feshbach resonances[39] to strengthen the on-site interaction. With periodic driving[40,41] or adiabatically tuning the lattice parameters[42], one may effectively couple neighbouring plaquettes with ring-exchange interactions to form larger systems. Our experiment offers a novel prospect for quantum simulation of topological phases[43,44] by engineering many-body interactions in ultracold atom systems, and will contribute to the future development of topological quantum computation[11,45–49].

Data availability. The data that support the plots within this paper and other findings of this study are available from the corresponding author upon reasonable request.

Received 20 December 2016; accepted 25 July 2017; published online 28 August 2017

References

1. Nielsen, M. & Chuang, I. *Quantum Computation and Quantum Information* (Cambridge Univ. Press, 2000).
2. Steane, A. M. Error correcting codes in quantum theory. *Phys. Rev. Lett.* **77,** 793–797 (1996).
3. Knill, E. Quantum computing with realistically noisy devices. *Nature* **434,** 39–44 (2005).
4. Kitaev, A. Fault-tolerant quantum computation by anyons. *Ann. Phys.* **303,** 2–30 (2003).
5. Wilczek, F. Quantum mechanics of fractional-spin particles. *Phys. Rev. Lett.* **49,** 957–959 (1982).
6. Han, Y.-J., Raussendorf, R. & Duan, L.-M. Scheme for demonstration of fractional statistics of anyons in an exactly solvable model. *Phys. Rev. Lett.* **98,** 150404 (2007).
7. Müller, M., Hammerer, K., Zhou, Y. L., Roos, C. F. & Zoller, P. Simulating open quantum systems: from many-body interactions to stabilizer pumping. *New J. Phys.* **13,** 085007 (2011).
8. Marcos, D. *et al*. Two-dimensional lattice gauge theories with superconducting quantum circuits. *Ann. Phys.* **351,** 634–654 (2014).
9. Paredes, B. & Bloch, I. Minimum instances of topological matter in an optical plaquette. *Phys. Rev. A* **77,** 023603 (2008).
10. Büchler, H. P., Hermele, M., Huber, S. D., Fisher, M. P. A. & Zoller, P. Atomic quantum simulator for lattice gauge theories and ring exchange models. *Phys. Rev. Lett.* **95,** 040402 (2005).
11. Aguado, M., Brennen, G. K., Verstraete, F. & Cirac, J. I. Creation, manipulation, and detection of Abelian and non-Abelian anyons in optical lattices. *Phys. Rev. Lett.* **101,** 260501 (2008).
12. Weimer, H., Müller, M., Lesanovsky, I., Zoller, P. & Büchler, H. P. A Rydberg quantum simulator. *Nat. Phys.* **6,** 382–388 (2010).
13. Wiese, U.-J. Ultracold quantum gases and lattice systems: quantum simulation of lattice gauge theories. *Ann. Phys.* **525,** 777–796 (2013).
14. Tagliacozzo, L., Celi, A., Orland, P., Mitchell, M. W. & Lewenstein, M. Simulation of non-Abelian gauge theories with optical lattices. *Nat. Commun.* **4,** 3615 (2013).
15. Banerjee, D. *et al*. Atomic quantum simulation of U(N) and SU(N) non-Abelian lattice gauge theories. *Phys. Rev. Lett.* **110,** 125303 (2013).
16. Zohar, E., Cirac, J. I. & Reznik, B.Quantum simulations of lattice gauge theories using ultracold atoms in optical lattices . *Rep. Prog. Phys.* **79,** 014401 (2016).
17. Lu, C.-Y. *et al*. Demonstrating anyonic fractional statistics with a six-qubit quantum simulator. *Phys. Rev. Lett.* **102,** 030502 (2009).
18. Pachos, J. K. *et al*. Revealing anyonic features in a toric code quantum simulation. *New J. Phys.* **11,** 083010 (2009).
19. Feng, G., Long, G. & Laflamme, R. Experimental simulation of anyonic fractional statistics with an nmr quantum-information processor. *Phys. Rev. A* **88,** 022305 (2013).
20. Park, A. J., McKay, E., Lu, D. & Laflamme, R. Simulation of anyonic statistics and its topological path independence using a seven-qubit quantum simulator. *New J. Phys.* **18,** 043043 (2016).
21. Barreiro, J. T. *et al*. An open-system quantum simulator with trapped ions. *Nature* **470,** 486–491 (2011).
22. Jiang, L. *et al*. Anyonic interferometry and protected memories in atomic spin lattices. *Nat. Phys.* **4,** 482–488 (2008).
23. Jaksch, D., Bruder, C., Cirac, J. I., Gardiner, C. W. & Zoller, P. Cold bosonic atoms in optical lattices. *Phys. Rev. Lett.* **81,** 3108–3111 (1998).
24. Bloch, I., Dalibard, J. & Zwerger, W. Many-body physics with ultracold gases. *Rev. Mod. Phys.* **80,** 885–964 (2008).
25. Simon, J. *et al*. Quantum simulation of antiferromagnetic spin chains in an optical lattice. *Nature* **472,** 307–312 (2011).
26. Fukuhara, T. *et al*. Quantum dynamics of a mobile spin impurity. *Nat. Phys.* **9,** 235–241 (2013).
27. Nascimbène, S. *et al*. Experimental realization of plaquette resonating valence-bond states with ultracold atoms in optical superlattices. *Phys. Rev. Lett.* **108,** 205301 (2012).
28. Aidelsburger, M. *et al*. Realization of the Hofstadter Hamiltonian with ultracold atoms in optical lattices. *Phys. Rev. Lett.* **111,** 185301 (2013).
29. Miyake, H., Siviloglou, G. A., Kennedy, C. J., Burton, W. C. & Ketterle, W. Realizing the Harper Hamiltonian with laser-assisted tunneling in optical lattices. *Phys. Rev. Lett.* **111,** 185302 (2013).
30. Jotzu, G. *et al*. Experimental realization of the topological Haldane model with ultracold fermions. *Nature* **515,** 237–240 (2014).
31. Fukuhara, T. *et al*. Spatially resolved detection of a spin-entanglement wave in a Bose–Hubbard chain. *Phys. Rev. Lett.* **115,** 035302 (2015).
32. Islam, R. *et al*. Measuring entanglement entropy in a quantum many-body system. *Nature* **528,** 77–83 (2015).
33. Dai, H.-N. *et al*. Generation and detection of atomic spin entanglement in optical lattices. *Nat. Phys.* **12,** 783–787 (2016).
34. Trotzky, S. *et al*. Time-resolved observation and control of superexchange interactions with ultracold atoms in optical lattices. *Science* **319,** 295–299 (2008).
35. Brown, R. C. *et al*. Two-dimensional superexchange-mediated magnetization dynamics in an optical lattice. *Science* **348,** 540–544 (2015).
36. Dutta, O. *et al*. Non-standard Hubbard models in optical lattices: a review. *Rep. Prog. Phys.* **78,** 066001 (2015).
37. Bakr, W. S. *et al*. Probing the superfluid-to-Mott insulator transition at the single-atom level. *Science* **329,** 547–550 (2010).
38. Sherson, J. F. *et al*. Single-atom-resolved fluorescence imaging of an atomic Mott insulator. *Nature* **467,** 68–72 (2010).
39. Chin, C., Grimm, R., Julienne, P. & Tiesinga, E. Feshbach resonances in ultracold gases. *Rev. Mod. Phys.* **82,** 1225–1286 (2010).
40. Eckardt, A., Weiss, C. & Holthaus, M. Superfluid–insulator transition in a periodically driven optical lattice. *Phys. Rev. Lett.* **95,** 260404 (2005).
41. Kitagawa, T., Berg, E., Rudner, M. & Demler, E. Topological characterization of periodically driven quantum systems. *Phys. Rev. B* **82,** 235114 (2010).
42. Trebst, S., Schollwöck, U., Troyer, M. & Zoller, P. d-wave resonating valence bond states of fermionic atoms in optical lattices. *Phys. Rev. Lett.* **96,** 250402 (2006).
43. Wen, X.-G. *Quantum Field Theory of Many-Body Systems* (Oxford Univ. Press, 2004).
44. Altman, E. & Auerbach, A. Plaquette Boson–Fermion model of cuprates. *Phys. Rev. B* **65,** 104508 (2002).
45. Kitaev, A. Anyons in an exactly solved model and beyond. *Ann. Phys.* **321,** 2–111 (2006).
46. Duan, L.-M., Demler, E. & Lukin, M. D. Controlling spin exchange interactions of ultracold atoms in optical lattices. *Phys. Rev. Lett.* **91,** 090402 (2003).
47. Zhang, C., Scarola, V. W., Tewari, S. & Das Sarma, S. Anyonic braiding in optical lattices. *Proc. Natl Acad. Sci. USA* **104,** 18415–18420 (2007).
48. Dusuel, S., Schmidt, K. P. & Vidal, J. Creation and manipulation of anyons in the Kitaev model. *Phys. Rev. Lett.* **100,** 177204 (2008).

49. Nayak, C., Simon, S. H., Stern, A., Freedman, M. & Das Sarma, S. Non-Abelian anyons and topological quantum computation. *Rev. Mod. Phys.* **80,** 1083–1159 (2008).

Acknowledgements

We thank A. J. Leggett, P. Zoller and B. Zhao for helpful discussions. This work was supported by the National Key R&D Program of China (2016YFA0301600), National Natural Science Foundation of China (91421305, 11521063), and the Chinese Academy of Sciences.

Author contributions

Y.-A.C., Z.-S.Y. and J.-W.P. initiated and designed this research project. H.-N.D., B.Y., A.R., X.-F.X. and Z.-S.Y. set up the experiment. H.-N.D., B.Y., A.R. and H.S. performed the measurement and analysed the data. All authors contributed to manuscript preparation. Z.-S.Y. and J.-W.P. supervised the whole project.

Additional information

Supplementary information is available in the online version of the paper. Reprints and permissions information is available online at www.nature.com/reprints. Publisher's note: Springer Nature remains neutral with regard to jurisdictional claims in published maps and institutional affiliations. Correspondence and requests for materials should be addressed to Z.-S.Y. or J.-W.P.

Competing financial interests

The authors declare no competing financial interests.